THE JOURNAL OF PHYSICAL CHEMISTRY A

Article

pubs.acs.org/JPCA

Trajectory Study of Energy Transfer and Unimolecular Dissociation of Highly Excited Allyl with Argon

Riccardo Conte,*[,†] Paul L. Houston,*[,‡,§] and Joel M. Bowman*[,†]

[†]Department of Chemistry and Cherry L. Emerson Center for Scientific Computation, Emory University, Atlanta, Georgia 30322, United States

[‡]School of Chemistry and Biochemistry Georgia Institute of Technology, Atlanta, Georgia 30332, United States

[§]Department of Chemistry and Chemical Biology, Cornell University, Baker Laboratory, Ithaca, New York 14852, United States

ABSTRACT: The influence of rotational excitation on energy transfer in single collisions of allyl with argon and on allyl dissociation is investigated. About 90 000 classical scattering simulations are performed in order to determine collision-induced changes in internal energy and in allyl rotational angular momentum. Dissociation is studied by means of about 50 000 additional trajectories evolved for the isolated allyl under three different conditions: allyl with no angular momentum ($J = 0$); allyl with the same microcanonically sampled initial conditions used for the collisions (J^*); allyl evolving from the corresponding exit conditions after the collision. The potential energy surface is the sum of an intramolecular potential and an interaction one, and it has already been used in a previous work on allyl−argon scattering (Conte, R.; Houston, P. L.; Bowman, J. M. *J. Phys. Chem. A* **2013**, *117*, 14028−14041). Energy transfer data show that increased initial rotation favors, on average, increased relaxation of the excited molecule. The availability of a high-level intramolecular potential energy surface permits us to study the dependence of energy transfer on the type of starting allyl isomer. A turning point analysis is presented, and highly efficient collisions are detected. Collision-induced variations in the allyl rotational angular momentum may be quite large and are found to be distributed according to three regimes. The roles of rotational angular momentum, collision, and type of isomer on allyl unimolecular dissociation are considered by looking at dissociations times, kinetic energies of the fragments, and branching ratios. Generally, rotational angular momentum has a strong influence on the dissociation dynamics, while the single collision and the type of starting isomer are less influential.

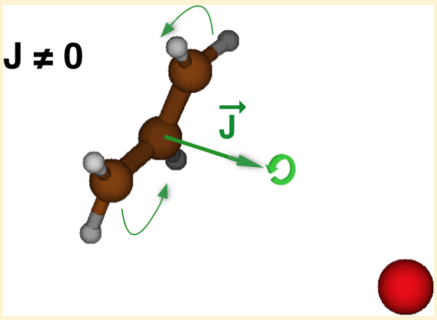

I. INTRODUCTION

Allyl radicals are important intermediates in atmospheric chemistry and combustion of hydrocarbons.[1,2] Previous photodissociation experiments[3,4] and quasi-classical trajectory (QCT) simulations have focused on rotationally cold allyl by investigating both unimolecular dissociation[5,6] and energy transfer in collisions with argon.[7] However, the role of internal rotation is of great interest and should not be overlooked.[8−10] Allyl radicals with high angular momentum can be the result of recombination reactions ($H + C_3H_4$, $CH_3 + C_2H_2$) that occur at large impact parameters, or the outcome of molecular dissociation of allyl-Br or allyl-I[11,12] where, due to conservation of angular momentum, the ejection of the heavy halogen atom imparts considerable rotation to allyl. In the well-known two-step Lindemann mechanism,[13,14] rotation may strongly affect both steps, i.e. both the collisional energy transfer and the subsequent unimolecular dissociation dynamics of the excited allyl radical.

To gain a deeper understanding of energy transfer and dissociation processes, experiments (see, for instance, refs 15−30) and theoretical studies (see, for instance, refs 31−44) of collisions between an excited target molecule and an inert collider are fundamental. With respect to the isolated molecule, the projectile can either stabilize the molecule as the result of a transfer of energy from vibrational or rotational degrees of freedom to translation (V → T and R → T) or favor dissociation if, on the contrary, the net transfer is directed from translational to internal energy.[45,46]

Many different aspects can influence the energy transfer. The nature of the bath gas, the collision energy, and the internal excitation of the molecule are all critical. Master equations, which describe the temperature and pressure dependence of rate coefficients, strongly depend on the accuracy of the evaluated energy transfer. However, even if exact quantum scattering calculations have been perfomed for some systems,[47−49] they become not practical when dealing with molecules made of more than four or five atoms. Simulations for larger systems are performed by means of (quasi-)classical trajectory propagation, an approach that is quite reliable, especially in the case of highly excited targets. It should be pointed out that classical mechanics provides an approximation to exact quantum mechanics, and a careful assessment of the simulation conditions has to be performed before considering the results of classical simulations as reliable. In this specific

Received: June 22, 2014
Revised: August 4, 2014
Published: August 12, 2014

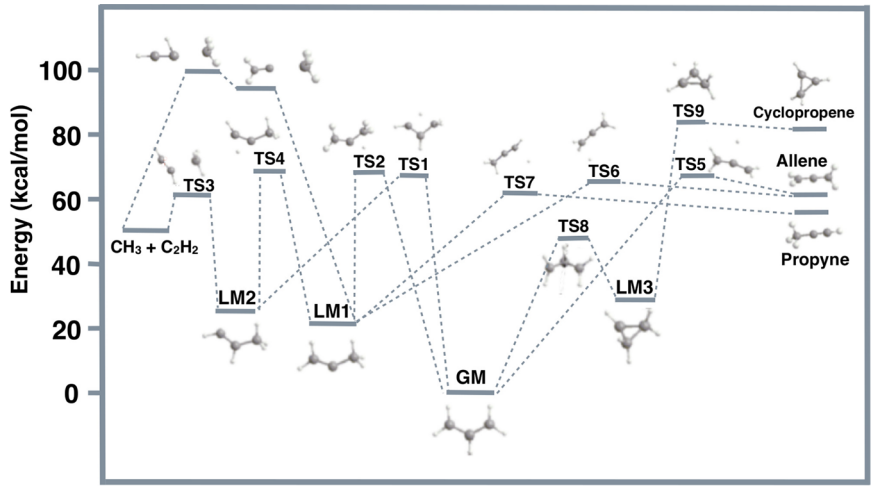

Figure 1. Schematic plot of the allyl intramolecular potential energy surface.

case, internal energy is well above the excitation energies necessary to open all chemically relevant dissociation channels, the density of states is high and quantum tunneling effects are not likely to play a major role. Moreover, another drawback of classical simulations, i.e. zero point leakage, is highly improbable. Even though methods have been proposed to correct for it,[50,51] they appear not to be necessary for high internal energy simulations.

The reliability of the potential energy surface (PES) on which nuclei move is another aspect of major importance for accurate scattering calculations. Recently, collision studies have been carried out by means of direct dynamics.[52−54] The trajectory is evolved by calculating at each step the exact full-dimensional quantum mechanical *ab initio* gradient necessary to carry on the subsequent step. This approach, when feasible, has the advantage of not requiring a fit to the data points, and no error is introduced relative to the *ab initio* method chosen. However, direct-dynamics methods are limited to computationally cheap and fast electronic structure methods. They are also not amenable to the investigation of rare phenomena like highly efficient collisions (HEC), which require a substantial number of trajectories for their detection.

In a more common approach, the full-dimensional PES is rigorously rearranged as a sum of an intramolecular potential and an intermolecular one. For the former, models based on harmonic or Morse-like oscillators have often been used, while recently a permutationally invariant (PI) intramolecular PES has been employed for collisions of allyl with argon;[7] for the latter, simple sum-of-pair potentials are usually fitted to a limited set of electronic energies with good precision.[55,56] Attempts to increase accuracy in intermolecular potentials have been undertaken both by refining the fits on the basis of high-resolution spectroscopic data for molecular complexes[57] and by introducing a new kind of permutationally invariant fit specifically designed for interaction potentials.[58] This last approach necessitates a larger number of *ab initio* energies, but it is based on linear parameter fitting. It is characterized by a lower rms error than the pairwise fit, and it is capable to describe also multibody contributions that are not negligible at the short separation distances experienced along the repulsive wall.

Dissociation of highly excited molecules can be investigated by determination of branching ratios, dissociation times, and kinetic energy distribution of the fragments. Trajectory simulations of rotationally excited allyl are expected to show the effect of the centrifugal barrier which hinders dissociation and related phenomena. Experimentally, the effect was detected for the H-elimination channels, even if in those experiments allyl had a lower internal excitation than in our simulations.[11,12] The allyl intramolecular PES[5] used in this work presents various dissociation channels: some of them lead to hydrogen elimination and formation of cyclopropene, allene, or propene. Two more are characterized by methyl elimination with acetylene formation. Dissociation times can be calculated by fitting data of the time-evolved allyl population. Moreover, from kinetic energy distributions of fragments it is possible to evaluate how the initial energy has been partitioned between the internal energy of the fragments and the relative motion.

The main goals of the paper are represented by the study of collisions of rotationally hot allyl with argon, and by the investigation of the role of angular momentum in both collisions and allyl unimolecular dissociation. The high-level PES employed also allows the role of the starting isomer to be assessed.

In this paper we present trajectory results for the energy transfer and unimolecular dissociation of allyl with argon. Section II highlights the main features of the PES used in this work and describes the methodology adopted in trajectory simulations. In Section III, the main results for energy transfer, variation of rotational angular momentum, and unimolecular dissociation are presented. The final section of the paper is devoted to a discussion about separability between rotational and vibrational energy, microcanonical sampling, and importance of rotational excitation in allyl dissociation.

In an upcoming paper,[59] we will use the trajectory results reported here to develop a soft-sphere model which helps to understand the physical mechanism underlying excitation and de-excitation in collisions. Trajectories have been performed at the microcanonical level, and this has permitted us to construct the model by taking explicitly into account conservation laws. The joint probability $(P(\Delta E, \Delta J))$ obtained by trajectory simulations can be fitted by the model without the need to rely on a separation approximation or ad hoc parameters and fitting formulae.

dx.doi.org/10.1021/jp5062013 | J. Phys. Chem. A 2014, 118, 7742−7757

II. POTENTIAL ENERGY SURFACE AND DESCRIPTION OF TRAJECTORY METHOD

Potential energy surfaces of radicals often have multiple reaction paths, as can be seen in the case of allyl (Figure 1). Isomerization can also be argued to be more facile in a radical species. So the radical nature of allyl makes the intramolecular potential more interesting. At the intermolecular level, when focusing on collisions with an inert gas (argon), the main effect of the radical species consists in stronger interactions and a deeper interaction well.

The global Ar-allyl PES can be expressed as the sum of an intramolecular potential for the allyl and an interaction potential between the argon and the allyl. A schematic plot of the high-level intramolecular potential is reported in Figure 1, while energy values of the relevant points on the surface are presented in Table 1. A complete list of vibrational frequencies

Table 1. Energy Values of the Allyl PES Relative to the Global Minimum (kcal/mol)

stationary point	energy
GM	0
LM1	20.4
LM2	25.0
LM3	29.5
TS1	69.6
TS2	70.5
TS3	62.5
TS4	70.9
TS5	69.4
TS6	66.4
TS7	63.5
TS8	51.9
TS9	86.7
HCCH + CH_3	52.4
allene + H	62.9
propyne + H	58.4
cyclopropene + H	83.5

can be found in a previous work.[5] For the goals of this work, we focus on the presence of four stable isomers, indicated henceforth (in increasing energy order) as GM (HCH_2–CH–CH_2), LM1 (HCH_3–C–CH_2), LM2 (HCH_3–CH–CH), and LM3 for the triangular conformer. Moreover, the surface is able to describe various dissociation paths divided into two main groups, according to the type of fragment eliminated. There are two pathways for methyl elimination starting from GM. One involves a hydrogen 1,3 shift. The other one involves hydrogen 1,2 shifts. After a first 1,2 hydrogen shift, the path proceeds either through LM1 and finally dissociates via the vinylidene channel or by means of a second 1,2 hydrogen shift to give LM2 and finally dissociates. Experiments[4] have distinguished between these channels by starting with a GM isomer that has a deuterium in place of the central H atom. The other dissociation paths eliminate hydrogen to yield propyne, allene, or cyclopropene.

The intermolecular Ar–allyl potential has been approximated by a sum of pairwise potentials between the argon atom and each H or C atom of the allyl.[56] Details have been reported in ref 7. In Figure 2 we present contour plots of the attractive wells for the interaction potentials of argon with the four stable isomers.

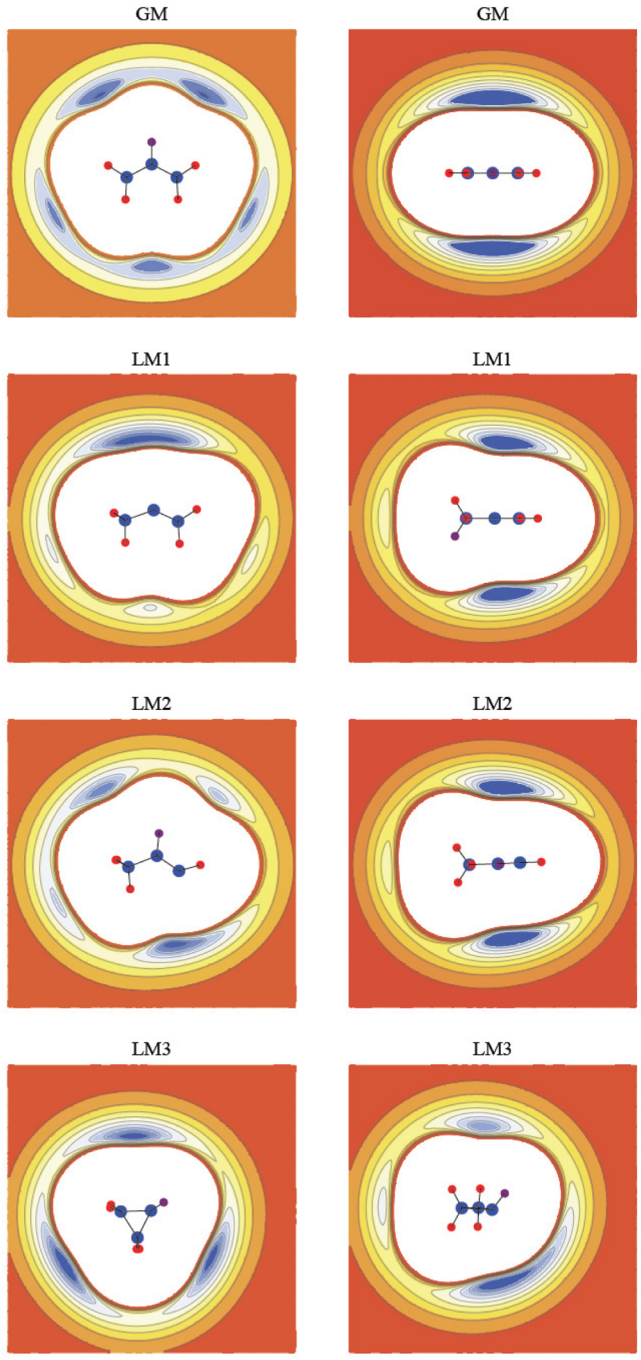

Figure 2. Contour plots of the attractive well of the Ar-allyl interaction potential for the four allyl isomers. On the left column the carbon atoms are in the plane of the page; on the right column they are positioned in a plane perpendicular to the page. The red contours are at a potential energy of zero, while the darkest blue contours are at a potential of −200 cm^{-1}. The contour interval is 25 cm^{-1}.

Trajectories were run under different conditions, according to the questions they were intended to address. The effects of initial angular momentum, collision, and different starting isomer have been investigated by means of four groups of trajectories which were performed for each different stable isomer: (1) trajectories for isolated allyl and no rotation (henceforth called "J = 0, no-coll"); (2) collisional trajectories for argon colliding with microcanonically sampled rotationally excited allyl ("J*, coll"); (3) trajectories for isolated allyl,

dx.doi.org/10.1021/jp5062013 | J. Phys. Chem. A 2014, 118, 7742–7757

starting from the same initial conditions used in batches at point (2) ("J^*, no-coll"); (4) trajectories for isolated allyl but initiated from the final conditions emerging from batches of type (2) ("J, post-coll").

By mimicking the Lindemann mechanism, the trajectories involving the approach and retreat of the Ar ("J^*, coll") were run separately from the trajectories that described the subsequent unimolecular evolution to products ("J, post-coll"). This is justified by the observation that the collision time is much shorter (by a factor of 10 or more, depending on the relative energy) than the time for dissociation (typically 10−100 ps for rotating allyl). The number of trajectories evolved allowed us to obtain reliable statistics for product analysis. For case (2) a larger number of trajectories have been run for use also in our energy transfer model.[59] A summary of the number of trajectories run is reported in Table 2.

Table 2. Number of Trajectories Used for Different Simulations in This Study

starting isomer	J = 0, no-coll	J^*, coll	J^*, no-coll	J, postcoll
GM	18 627	29 878	6000	5932
LM1	2500	26 319	2500	2500
LM2	2499	21 139	2000	1999
LM3	2341	23 717	2500	2500

All trajectory calculations, for all four allyl isomers, were performed setting the total internal energy to 157.2 kcal/mol above the GM electronic energy. This energy was chosen because it was used for both experiments[3,4] and previous trajectory calculations on isolated allyl[7] and because it is high enough to access all of the observed dissociation channels.

All trajectories concerning the evolution of isolated allyl (case (1), (3), or (4) above) were run on the PI PES until either the allyl dissociated or until 200 000 time steps of 0.12 fs (24 ps in total) had elapsed. Final conditions permitted characterization of products by angular momentum, dissociation time, exit channel, and kinetic energy. This analysis was performed by means of a program which automatically divided the final configurations into different categories.

Collisional trajectories (case (2) above) were performed at a collisional energy of 10 kcal/mol (or 3497.6 cm^{-1}). Additional trajectories for rotating allyl were run at E_{coll} = 2 kcal/mol (or 699.5 cm^{-1}) and directly compared to previous data for nonrotating allyl. A microcanonical sampling (J^*) was performed for the allyl initial conditions by giving atoms random velocities.[60] After subtraction of translational—and for J = 0 simulations also rotational—motion, the remaining kinetic energy was scaled to the selected value. The starting geometry was chosen to be that of one of the isomers. The initial orientation of the allyl with respect to the argon was varied by random rotation through Euler angles. At the beginning of the simulation the allyl was free to sample the phase space without interaction. A small batch of trajectories was run to determine the maximum impact parameter (b_{max} = 11.5 au) using the simulation time as a guide, as described in our previous work.[7]The impact parameter for the main set of trajectories was then selected from values between 0 and b_{max} according to the distribution

$$dP(b)/db = 2\pi b/\pi b_{max}^2 \quad (1)$$

and using a Monte Carlo sampling to generate it from a uniform distribution of random numbers (rnd) in the interval (0,1).

$$b = b_{max}\sqrt{rnd} \quad (2)$$

The allyl−argon distance was initially set to 15 au to ensure that the initial interaction energy was negligible. A collisional trajectory was stopped in the case of dissociation or when the argon returned 16 au away from the nearest allyl atom. Trajectories were discarded and not considered for energy transfer and angular momentum analysis if they dissociated before the collision was terminated or after visiting an unphysical region where the PI intramolecular PES was not fitted to enough *ab initio* points. In all the collisional simulations performed, a negligible fraction of the trajectories (roughly 0.15%) entered these unphysical regions of the PES and were discarded. The frequency of interruption due to dissociation depends on the average duration of the simulation (i.e., the collision energy), on the presence of rotational angular momentum, and on the starting isomer. These two last aspects are related to the height of the barrier to dissociation. By adding angular momentum, dissociation is hindered, as we will discuss in the paper. Isomers LM1, LM2, and LM3 have lower barriers to overcome (see Figure 1) than GM. At E_{coll} = 2 kcal/mol, calculations were performed only for the GM isomer. The dissociation fractions are 7.4% for J = 0 and 1.1% for J^*. At E_{coll} = 10 kcal/mol (J^*), a different percentage of dissociated trajectories is found for each isomer (GM: 0.4%; LM1: 15.5%; LM2: 36.3%; LM3: 1.3%). This is in agreement with data of dissociation times and percentage of nonreactive trajectories of the isolated radical which will be presented in the unimolecular dissociation section. Collisional trajectories allowed us to characterize rigorously the total energy transfer ΔE and the change in internal angular momentum ΔJ.

III. RESULTS

Collisional Energy Transfer and Variation in Rotational Angular Momentum. The first step in the Lindemann mechanism involves energy transfer between the colliding species. We have run batches of several thousand collisions (see column "J^*, coll" in Table 2) to investigate energy transfer. The average total energy transfer $\langle\Delta E\rangle$ was calculated as an average over trajectory contributions

$$\langle\Delta E\rangle = \frac{1}{N_{traj}}\sum_{i=1}^{N_{traj}}\Delta E_i \quad (3)$$

The average in eq 3 is referenced to the hard sphere collision rate Z_{HS} evaluated at b_{max},[52]

$$Z_{HS} = \pi b_{max}^2\sqrt{8k_BT_{bath}/\pi\mu} \quad (4)$$

The value of Z_{HS} is evaluated from eq 4 by considering the bath temperature related to the collisional energy $E_{coll} = 2k_BT_{bath}$ as suggested in refs 31 and 61. $\mu \approx 36\,900$ au is the reduced mass for allyl−argon. At the collision energy of 10 kcal/mol in our simulations, $Z_{HS} = 18.8 \times 10^{-10}$ cm^3 $molecule^{-1}$ s^{-1}.

The physical observable we report is the average energy transfer rate. It is dependent on neither the b_{max} value (provided it is big enough to include all relevant interactions) nor on the collision rate, and it is defined as the product of the average energy transfer and the corresponding collision rate

dx.doi.org/10.1021/jp5062013 | J. Phys. Chem. A 2014, 118, 7742−7757

Table 3. Energy Transfer Data for Argon−Allyl Collisions with Allyl Starting in Different Isomer Geometries[a]

E_{coll} = 10 kcal/mol	$\langle E \rangle$	$r_{\Delta E}$	$\langle \Delta E^d \rangle$	HEC (thr.)	% HEC	% $\langle \Delta E^d \rangle$
GM	−516.8	−9715.8	−1376.3	−6881.5	1.8	25.1
LM1	−588.3	−11 060.0	−1465.8	−7329.0	1.8	22.9
LM2	−605.5	−11 383.4	−1450.6	−7253.0	1.9	23.1
LM3	−346.4	−6512.3	−1077.0	−5383.0	1.7	25.1

[a]The columns, in order, refer to type of isomer; average total energy transfer (cm^{-1}); energy transfer rate (10^{-10} cm^{-1} cm^3 $molecule^{-1}$ s^{-1}); average energy transfer down (cm^{-1}); energy transfer down threshold for HEC (cm^{-1}); percentage of highly efficient collisions; fraction of energy transfer down due to highly efficient collisions.

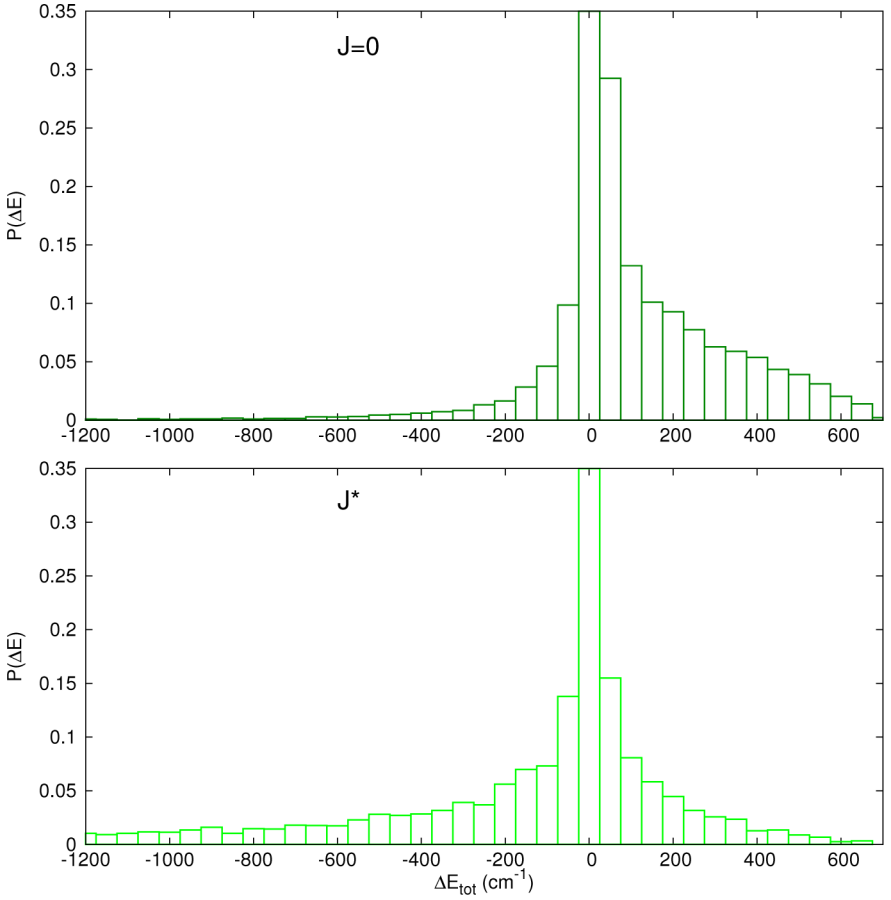

Figure 3. Total energy transfer histograms. Allyl is initially set in the GM configuration. The collision energy is 2 kcal/mol. In the upper panel, allyl has no initial angular momentum (J = 0). In the lower panel, allyl is rotationally excited after microcanonical sampling (J*). Elastic bins have been normalized to 1, but truncated in the figure.

Table 4. Comparison of Energy Transfer Data for Collisions at E_{coll} = 2 kcal/mol for Allyl with and without Initial Rotational Excitation, Starting from GM Geometry[a]

2 kcal/mol	$\langle \Delta E \rangle$	$r_{\Delta E}$	$\langle \Delta E^d \rangle$	HEC (thr.)	% HEC	% $\langle \Delta E^d \rangle$
GM (J = 0)	75.6	695.2	−121.9	−609.5	0.9	39.5
GM (J*)	−306.6	−2820.7	−676.6	−3383.0	1.8	23.2

[a]Column labels are the same as those in Table 3. Energy values are in cm^{-1}. The energy transfer rate is in 10^{-10} cm^{-1} cm^3 $molecule^{-1}$ s^{-1}.

$$r_{\Delta E} = Z_{HS}\langle \Delta E \rangle \quad (5)$$

Table 3 presents the main data relative to the energy transfer. At first sight, some features may be readily noticed and are worth being examined more in detail. First, the average energy values are fairly big. The average total energy transfer is 10−17% of the collisional energy, and it is negative for all isomers even if the collisional energy is quite high. Second, GM, LM1, and LM2 isomers seem to have similar energy transfer values, while LM3 differs to a greater extent. Third, in collisions involving rotationally excited allyl as well as in the previously reported collisions for J = 0,[7] we are able to detect a set of highly efficient collisions which contribute substantially to the energy transfer down. HEC are defined (according to Clary's metric) as collisions contributing with an energy transfer down bigger than a threshold value which is five times larger than the ensemble average energy down $\langle \Delta E^d \rangle$.[32]

To point out the effect of rotation on energy transfer, we additionally ran more than 7000 trajectories after micro-

dx.doi.org/10.1021/jp5062013 | J. Phys. Chem. A 2014, 118, 7742−7757

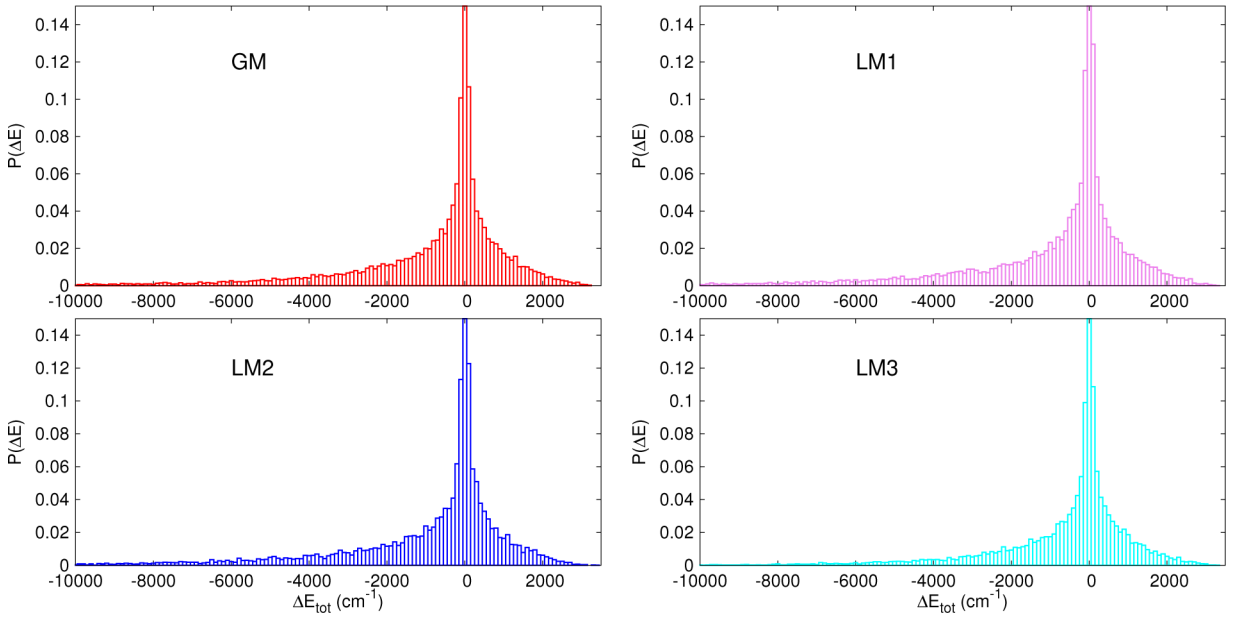

Figure 4. Total energy transfer histograms. Allyl (J^*) is initially set in the four different isomer configurations. The collision energy is 10 kcal/mol. $P(\Delta E)$ is in arbitrary units and set equal to 1 for the elastic bin (truncated in the picture). The bin width is 100 cm^{-1}.

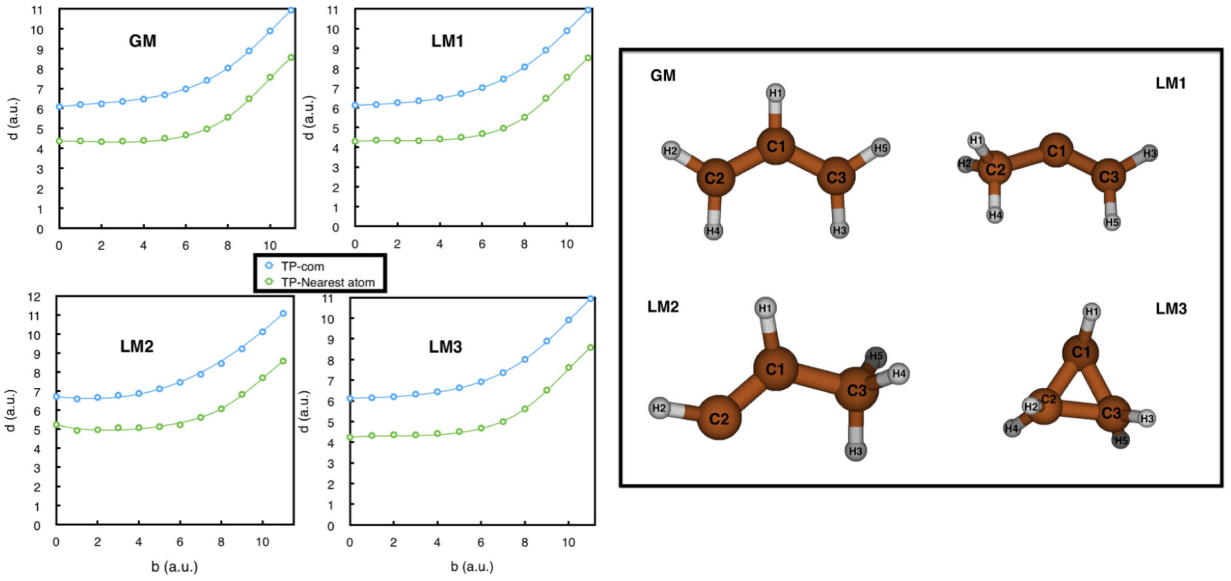

Figure 5. Turning point analysis. On the left, the four panels show for each isomer the average distance between the turning point and the allyl center of mass (cyan dots) and the nearest allyl atom (green dots) as a function of the impact parameter (b). On the right, the four isomers are pictorially reported together with atom labels.

canonical sampling (J^*) starting from GM geometry, at a relative energy of 2 kcal/mol, and with a maximum impact parameter of 12 au. The corresponding value of the hard sphere collision rate is $Z_{HS} = 9.2 \times 10^{-10}$ cm^3 $molecule^{-1}$ s^{-1}. This simulation permits a straightforward comparison with the data we have already published.[7] From Figure 3, one may clearly estimate that distributing the initial internal excitation between rotation and vibration (instead of forcing it into vibration only) has the effect of enhancing the energy transfer down. Both histograms in Figure 3 are limited for high ΔE by the value of the collision energy. More detailed data are collected in Table 4. In the case of nonrotating allyl, an increase in the relative energy was found to further excite the allyl by converting, on average, translational energy into rotational energy.[7] In the case of rotationally excited allyl, the efficiency of the collision in relaxing the radical increases as E_{coll} is shifted from 2 to 10 kcal/mol.

The microcanonical strong-collision limit and collision efficiency can be investigated on the basis of previous theoretical work on ergodic collision theory (ECT) by Nordholm and co-workers.[62−66] ECT is based on the assumption that when a collision complex is formed, a microcanonical equilibrium is generated before the two colliders separate.[63,67] The ECT limit is favored if the collision complex is a long-living one or in the presence of strong interactions. The ECT collision energy transfers were calculated by treating rotation and vibration classically. At E_{coll} = 2 kcal/mol, the gas temperature is T_{Ar} = 666.4 K and $\langle \Delta E^{ECT} \rangle$ = 3277

dx.doi.org/10.1021/jp5062013 | J. Phys. Chem. A 2014, 118, 7742−7757

cm^{-1}; at E_{coll} = 10 kcal/mol, the argon temperature is T_{Ar} = 3332 K and $\langle \Delta E^{ECT} \rangle$ = 679 cm^{-1}. The "weak collision effect" can be summarized in a collision efficiency β_E obtained as the ratio between the trajectory energy transfer and the ECT one. At E_{coll} = 2 kcal/mol, β_E = 0.094, and at E_{coll} = 10 kcal/mol, β_E = 0.76. The calculated efficiencies are consistent with data reported for other collisional systems.[65,66]

Another aspect of energy transfer that we examine is the role of different isomers. This is a topic which is quite new with respect to previous work in the literature and one that we are able to investigate because of the high-level intramolecular PES available. Figure 4 reports histograms for the total energy transfer in collisions performed at E_{coll} = 10 kcal/mol for J^* allyl starting in the four different isomer geometries. Even if the LM3 distribution is less prominent into the negative energy transfer territory, histograms are quite similar and the isomer dependence does not show a substantial impact if compared to the effect of angular momentum addition. The feature is also reproduced by our upcoming model,[59] which can fit pretty well the probability distributions for the different isomers by using the same set of physical parameters. These similar distributions call into question if there are correspondences at the microscopic level of the collisions.

To gain better knowledge of the role of the isomers in energy transfer, we present a turning point (TP) analysis. A TP is defined as the configuration of nearest approach between the argon and the allyl center of mass (com). The interaction can be an impulsive one, or the collider can start hovering around the molecule, resulting in a longer interaction. In the former case, there is a single approach and a single turning point is detected. In the latter, multiple turning points can be identified but only the one with the shortest distance is considered in the analysis. In collisions run at E_{coll} = 10 kcal/mol, it turned out that more than 90% of interactions were impulsive ones, independent of the particular starting isomer. Figure 5, in the four left-hand panels, shows the average TP−com distance (cyan dots) as a function of the impact parameter. The same figure reports the corresponding average distance between the argon and the nearest allyl atom (green dots). The four sets of curves for the different isomers are quite similar, with slopes increasing with the impact parameter and a minimum TP−com distance of about 6−7 au. Only LM2 shows slight differences at low impact parameters. This similarity prompted us to look at the type of allyl atom (labeled in the right panel of Figure 5) involved in the approach. The fraction of nearest approaches for the type of atom is reported in Table 5 and leads to the discovery that in all isomers the huge majority of nearest approaches is between the argon and a hydrogen atom. We recall that the interaction potential has been constructed as a sum of Ar−H and Ar−C pairwise potentials, so on the basis of these data, in a large majority of cases it is just the Ar−H potential which is primarily important for the energy transfer, independent of the type of isomer. Furthermore, from a more detailed analysis that will be presented together with our model,[59] it turns out that, in contrast to what might be supposed from the two particular orientations chosen for Figure 2, the spherically averaged interaction potentials are nearly indistinguishable.

Table 6 reports data analyzed for the "J^*, coll" group and shows the correlation between the different isomers as a result of the collision. A large collision-induced mixing between the different isomers could be another possible reason for similar distributions, but data in Table 6 demonstrate that this is not the case. There is no large amount of scrambling between isomers, since more than 95% of the GM, LM1, or LM2 isomers go through the collision unaltered. The exception is LM3 that easily converts to GM because the two geometries are closely related by the breaking of a C−C bond.

Table 5. Percentage Distribution of Nearest Atoms at Turning Points for E_{coll} = 10 kcal/mol[a]

%	H1	H2	H3	H4	H5	C1	C2	C3
GM	17.8	19.7	18.3	18.5	19.5	1.5	2.3	2.4
LM1	16.8	16.7	20.4	16.7	20.2	6.6	0.1	2.5
LM2	19.4	23.3	15.5	14.5	14.7	3.0	9.1	0.5
LM3	20.4	18.2	18.4	18.3	18.8	3.1	1.3	1.5

[a]Atoms are labelled according to the right panel of Figure 5.

Table 6. Correlation (Percentage) between Different Isomers before and after Collision with Argon[a]

	GM	LM1	LM2	LM3
GM	**99.3**	0.4	0.5	**91.2**
LM1	0.1	**96.3**	0.3	0.4
LM2	0.1	1.3	**98.5**	0.1
LM3	0.1	–	–	6.9
Other	0.4	2.0	0.7	0.4

[a]The starting isomer is reported in columns, the exit isomer in rows. Into the group named "other" are collected the distorted geometries which cannot be classified as a particular isomer.

As a final feature of energy transfer associated with collisions, we focus on highly efficient collisions. They represent a small fraction of the total number of collisions (usually around 1−2%) but are interesting because they contribute relevantly to the average energy transfer down (see Tables 3, 4). HEC have been largely debated and have often been called "super-collisions". On the basis of Luther's KCSI experiments,[22,68] "supercollisions" have been demonstrated to have a statistical origin instead of being due to a special mechanism, as initially thought. For this reason we prefer to adopt the term "highly efficient collisions". Furthermore, HEC allow us to point out once more the importance of our high-level PES. In fact, these rare events are hardly detectable by means of direct-dynamics calculations and they are related to the distribution of energy among more or less active internal modes. From data analysis, we find that for all isomers, in simulations at E_{coll} = 10 kcal/mol, HEC are more frequent at small impact parameters while they become rare for values greater than 4.5/5.0 au. Just a few HEC are detected at very large impact parameters (b > 7.0 au) and for LM2 geometry only. These are long-time trajectories if compared with average ones, while HEC at small b values take place when the argon comes to a very short distance from a hydrogen atom. In a hard-sphere-like collision, the energy is impulsively transferred to the translational motion. HEC are detected in a bigger proportion when rotation is present, but their impact on the average energy transfer down is higher for J = 0. Figure 6 presents on a semilog plot the probability for the down wing of the energy transfer for the GM isomer. The two straight lines fit the "weak" and "strong" collision regimes (according to Troe's terminology) of the energy transfer down and define a crossover point. The crossover point is located at −344 cm^{-1}, and HEC (as defined by means of Clary's metric) are very far away in the tail of the "strong" collision regime.

dx.doi.org/10.1021/jp5062013 | J. Phys. Chem. A 2014, 118, 7742−7757

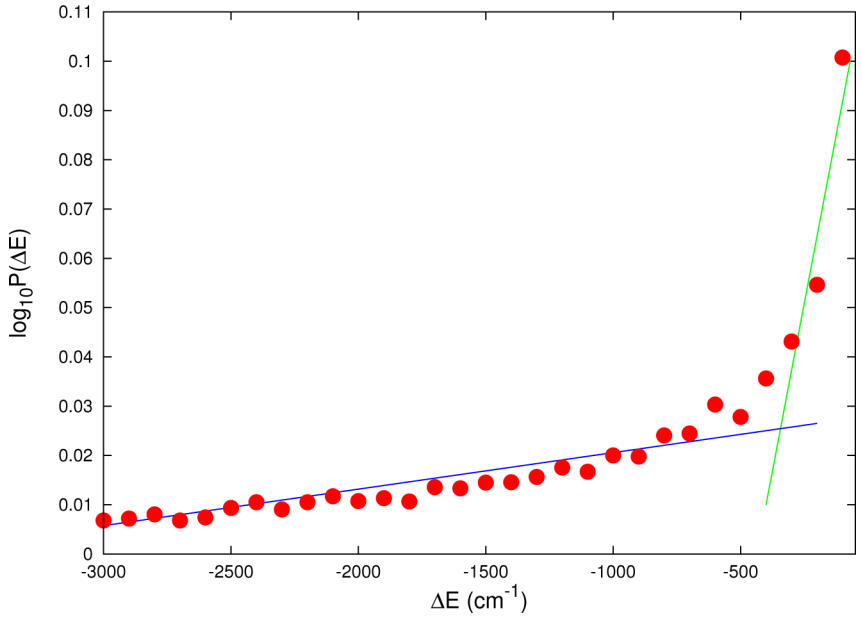

Figure 6. Analysis of energy transfer down. The two lines define two collisional regimes and intersect at the crossover point (-344 cm^{-1}). For the sake of clarity, the picture has been truncated at $\Delta E = -3000$ cm^{-1}. The energy bin width is 100 cm^{-1}.

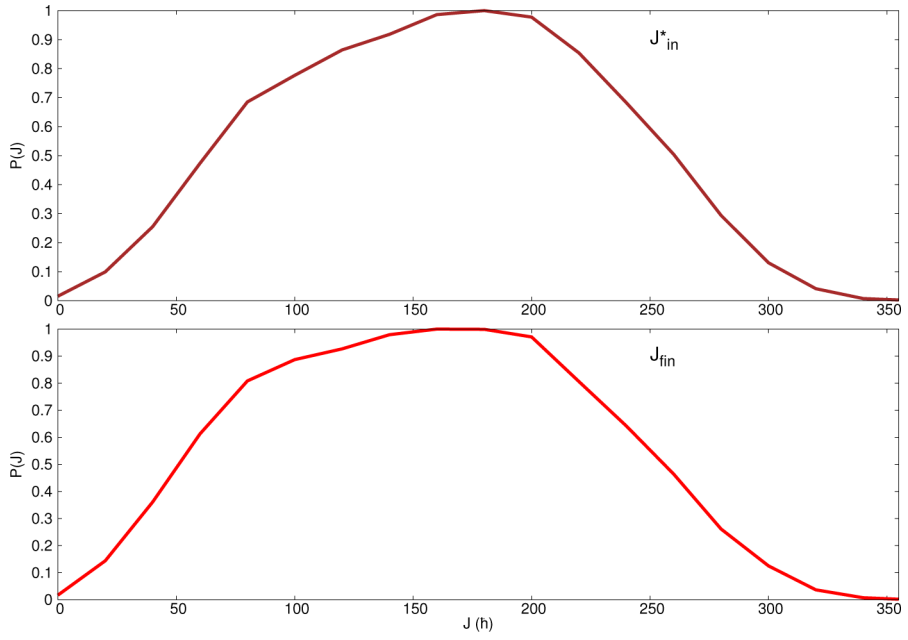

Figure 7. Comparison between allyl angular momentum distributions before and after the collision. The upper panel shows the initial distribution. The lower panel reports the final distribution. The initial geometry is GM, and the collision energy is 10 kcal/mol. Probabilities are normalized to 1 at the maximum value.

In the second part of this section, we focus on the collision-induced variation of allyl angular momentum. Figure 7 presents the initial (upper panel) and final (lower panel) rotational angular momentum distributions obtained from the batch of collisions with the allyl starting in GM geometry. The distribution is characterized by the initial average value $\langle J\rangle_{in} = 173.0\hbar$ with standard deviation $\sigma_{in} = 66.2\hbar$ and the final average value $\langle J\rangle_{fin} = 166.0\hbar$, $\sigma_{fin} = 67.1\hbar$. Rotational angular momentum distributions for the other isomers are quite similar, with LM3 averaging at a lower value ($\langle J\rangle_{in,LM3} = 131.4\hbar$, $\sigma_{in,LM3} = 43.3\hbar$). This can be explained by invoking the more compact triangular geometry of LM3. For all isomers, initial values are quite high. This demonstrates that the radical is prepared with high rotational excitation. On average, the collision decreases the value of the allyl angular momentum, which is compensated by an increase in the orbital one.

To look in more detail at the variation in rotational angular momentum, we analyze J_{fin} in collisions starting from GM geometry and with J_{in} centered around the value $J = 170\hbar$. This value was chosen because it is close to the average J_{in} value and to the maximum of the distribution (see Figure 7). Figure 8 shows in a semilog plot that in the large majority of collisions (about 80%) the change in internal angular momentum is small. Anyway, from Figure 8 it is possible to identify three

dx.doi.org/10.1021/jp5062013 | J. Phys. Chem. A 2014, 118, 7742−7757

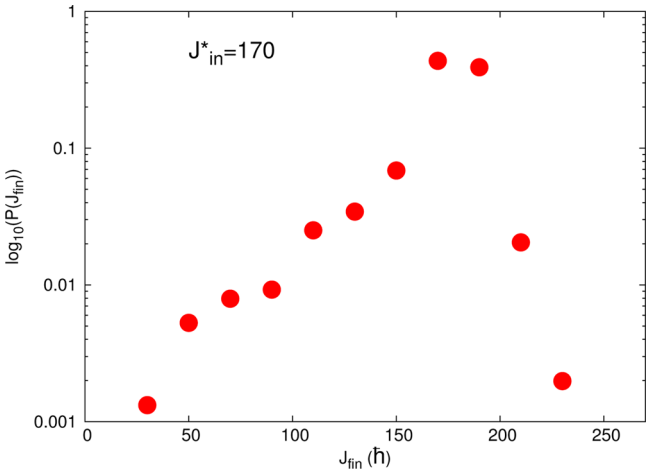

Figure 8. Distribution of allyl final angular momentum after collision with argon at E_{coll} = 10 kcal/mol, starting from a fixed initial angular momentum J_i = 170 ± 5$\hbar$. The width of J_f bins is 20$\hbar$. The allyl was initially set in GM geometry. The sum of the probabilities is equal to 1.

different regimes. Probabilities become very low and decrease at a fast pace for values of J_{fin} < 50$\hbar$. There is an intermediate regime with a milder slope for small or medium negative ΔJ variations. Finally, the decrement in probability is again very steep for collisions increasing the rotational angular momentum. The behavior of the two extreme regimes can be explained by invoking conservation of total (internal + orbital) angular momentum. In fact, on one hand, collisions with low impact parameters are generally not effective, since the orbital angular momentum is low and a very large ΔJ change would not conserve the total angular momentum. On the other hand, if the collision features a big impact parameter, the interaction is weak and the relative velocity is not deflected enough. In this case, there is little change in orbital angular momentum, so it is not possible to have a huge change in internal J. As |ΔJ| increases, a smaller and smaller fraction of trajectories may provide such a large variation in rotational angular momentum.

A way to point out the dependence of angular momentum transfer on the impact parameter is presented in Figure 9. Collisions with starting rotational angular momentum J^*_{in} = 200 ± 25$\hbar$ were collected according to their |ΔJ| values in bins

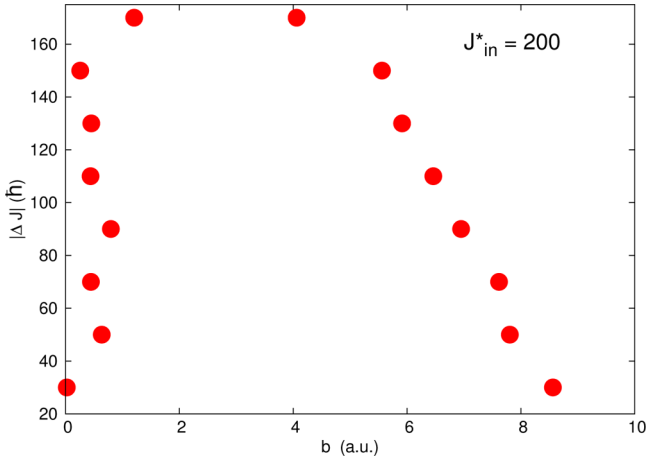

Figure 9. Minimum and maximum impact parameters (b) for |ΔJ| variations in collisions starting from J^*_{in} = 200 ± 25$\hbar$ and in GM geometry.

of width 20$\hbar$. The figure shows the extreme values (red dots) of the impact parameter in collisions that produced a given |ΔJ| variation of the allyl rotational angular momentum. There is a clear decrement in the maximum allowed impact parameter as |ΔJ| increases, while the minimum value starts increasing only for very high |ΔJ| values. The final outcome is that higher angular momentum variations are less probable, due to a restriction of the effective b-range. A similar feature is also found by our model.[59]

The dependence of big ΔJ values (>50$\hbar$) on the impact parameter has also been investigated and reported in Figure 10.

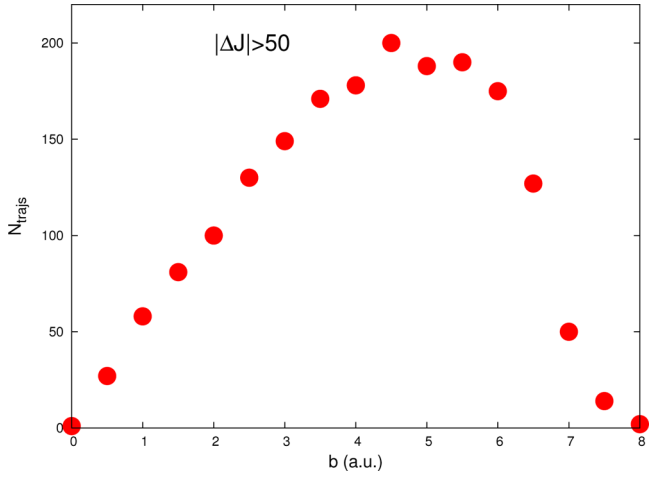

Figure 10. Distribution of trajectories with large change in rotational angular momentum (|ΔJ| > 50$\hbar$) as a function of the impact parameter. Data refer to the batch of collisions with allyl initially in GM geometry.

What we found in our analysis is as expected. The number of trajectories giving large variations in angular momentum (independently of the sign) is increasing for b values up to 4.5 au. The distribution starts dropping steeply as the impact parameter becomes bigger than 6 au and goes to zero at 8 au This once more demonstrates that if, on one hand, large impact parameters are expected to favor transfer of angular momentum, on the other, when the impact parameter is too big, the interaction is not strong enough to allow big changes in rotational angular momentum.

We have also investigated the role of the different isomers in affecting the rotational angular momentum change. Figure 11 presents on a semilog plot the probabilities of a change ΔJ in internal angular momentum for the four isomers. The plots show similar features with some differences in the extension of the tails of the distributions. In all cases, small changes in J are privileged. Slopes are steeper for positive rather than negative values of ΔJ. ΔJ ranges are narrower for GM and LM3. LM2 has some scattered distribution at very high and positive ΔJ, but the probability is so low that only very rare events (less than 0.1% of the total number of trajectories) are involved.

Finally, we have examined how highly efficient collisions are related to rotational angular momentum variations. If the allyl is given no rotation (J = 0), HEC are necessarily the result of an energy transfer from internal vibrations to the relative translational motion. Instead, when initial conditions are microcanonically sampled both rotational and vibrational energy can be responsible for HEC. One way to better understand the HEC mechanism is by looking at the ΔJ

dx.doi.org/10.1021/jp5062013 | J. Phys. Chem. A 2014, 118, 7742−7757

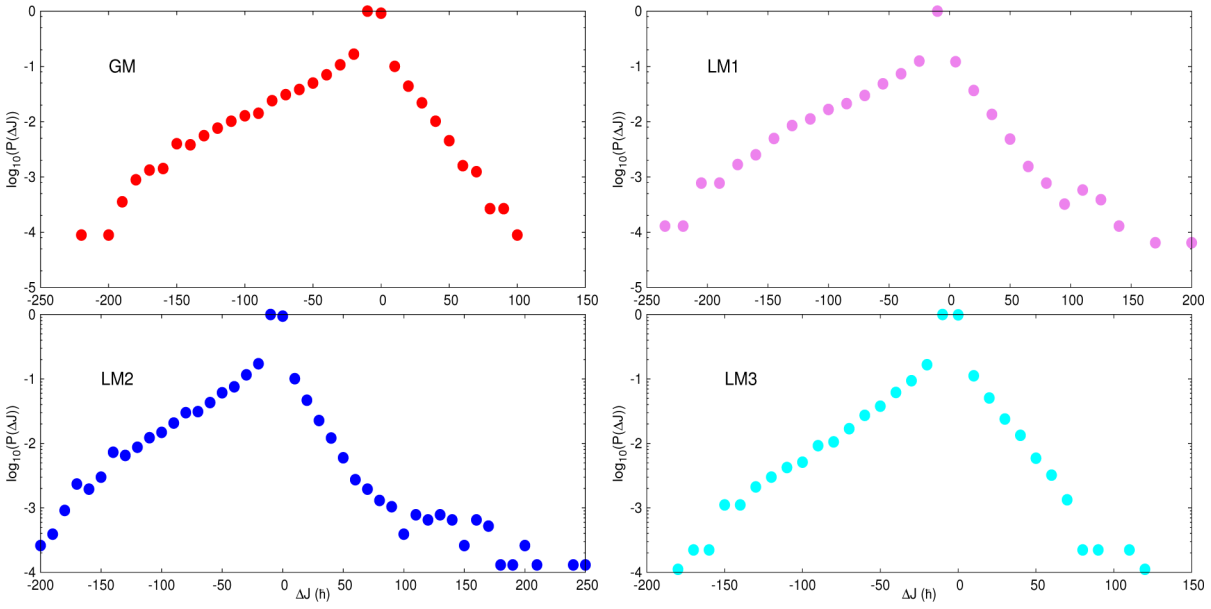

Figure 11. Distributions of the collision-induced change of allyl angular momentum for the four different isomers. The maximum of each distribution is normalized to 1.

distribution relative to HEC only. Figure 12 reports a peak not far from $\Delta J = -100\hbar$, and the probability remains non-

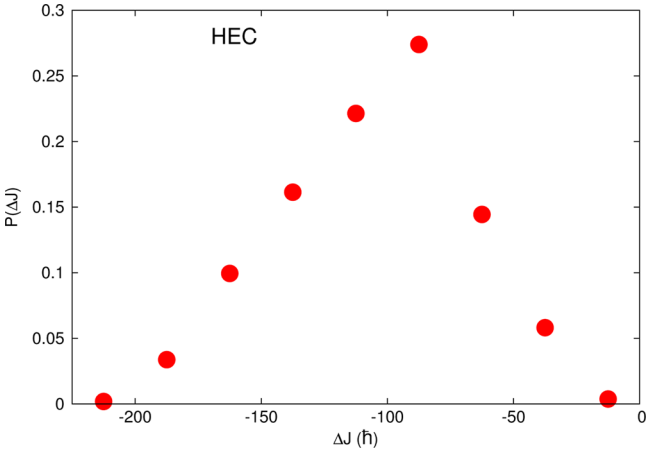

Figure 12. ΔJ distribution for HEC. The total probability is normalized to 1.

negligible down to a value of $-200\hbar$. Only about 7% of HEC feature a variation lower than 50 units, and only six HEC collisions (not reported in the Figure) are accompanied by small positive ΔJ values. These data demonstrate the large majority of HEC is characterized by a huge change in internal angular momentum, pointing to energy transfer from rotation to relative motion as the main cause for HEC.

Unimolecular Dissociation of Rotationally Excited Allyl. Another important topic we were able to investigate was how rotational excitation affects the dissociation of allyl. We studied the evolution of isolated allyl radicals which had been excited both rotationally and vibrationally. The total internal excitation was chosen to be 157.2 kcal/mol in agreement with previous work.[3−6] The role of the starting isomer is considered and so is the effect of the foregoing collision with argon, thus mimicking the second step in the Lindemann mechanism, which describes the dissociation of the excited molecule to products after the collisional energy transfer. For these purposes, we have run batches of trajectories divided into the three groups "$J = 0$, no-coll", "J*, no-coll", and "J, post-coll" (see Table 2), in the way described in Section II. Some of the simulations in the first group (those concerning the GM isomer) had already been performed and used to present results in a previous paper,[6] while new trajectories have been evolved for the four isomers and rotationally excited allyl. By comparison between the three groups, we can easily assess the role of angular momentum, collision, and starting isomer.

Figure 13 presents, on the top-left panel, the average magnitude of the angular momentum. Clearly, the group "$J = 0$, no-coll" is characterized by nonrotating allyl, while the other two groups reveal high angular momentum values. It is straightforward to conclude, by comparison of the green and orange histograms, that the collision, on average, had the effect of subtracting angular momentum from the radical.

A first consequence of the presence of angular momentum is pointed out in the top right panel. The variation in dissociation time with the addition of angular momentum to the starting isomer is striking. For instance, GM dissociation takes on average almost seven times as long for the rotationally excited allyl as for the $J = 0$ allyl. The effect is also greatly significant for the other isomers even if less marked. The collision, by decreasing the angular momentum by about 4−5%, decreases dissociation times in a similar proportion for GM and LM3, while no relevant change is detected for LM1 and LM2. Dissociation times have been calculated by an exponential fit to the distribution of undissociated molecules vs time.

The product distribution reflects the dissociation time, in that during the 24 ps time window for allyl evolution there are in general more nonreactive trajectories with rotation than without. This is clear from the bottom-left panel in Figure 13. The increment in the nonreactive trajectory percentage is quite large for GM and LM3 and smaller for LM1, while for LM2 it is irrelevant. The influence of the collision is negligible with some weak effect only for the LM3 isomer.

Finally, in the bottom-right panel, fragment kinetic energies are reported. The effect of angular momentum addition is

dx.doi.org/10.1021/jp5062013 | J. Phys. Chem. A 2014, 118, 7742−7757

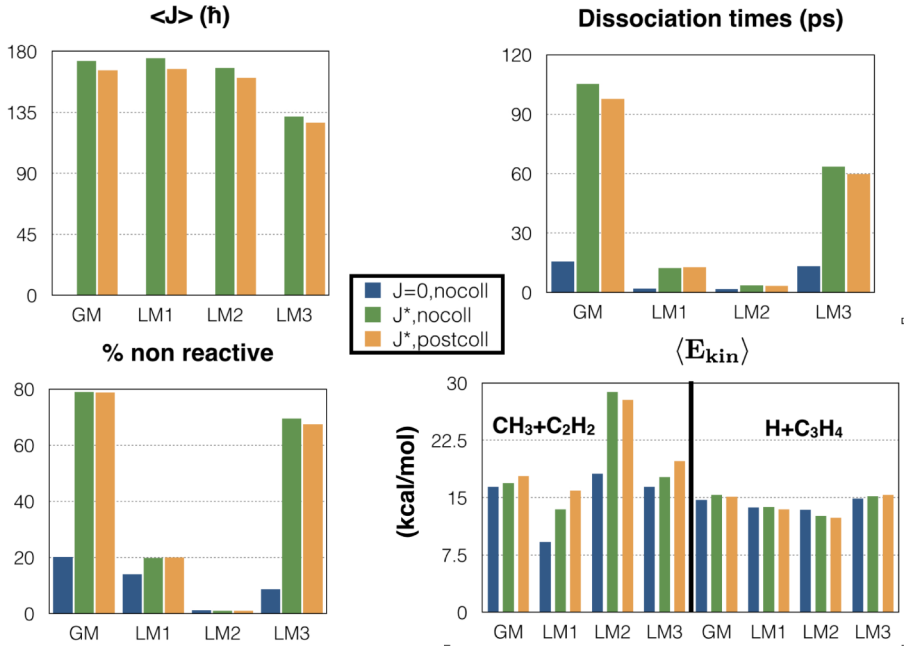

Figure 13. Dependence on the starting isomer. From top-left, moving clockwise: average angular momentum; dissociation times; average kinetic energy for moieties methyl + acetylene (left half) and hydrogen + C_3H_4 (right half); fraction of nonreactive trajectories. Results are reported for isolated nonrotating allyl (blue), isolated rotationally excited allyl (green), and rotationally excited allyl evolved after collision with an argon atom (orange).

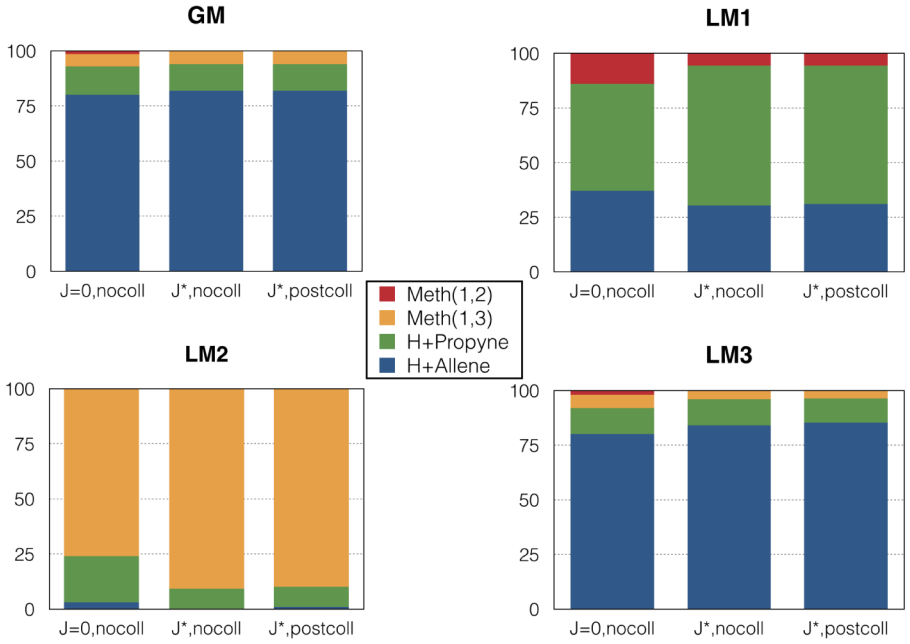

Figure 14. Branching ratios for the four isomers. In each panel, data are reported for three different cases: isolated allyl not rotating (left); isolated rotationally excited allyl (middle); rotationally excited allyl after a collision with argon (right).

minimal for the H-elimination channels, increasing slightly kinetic energies in the case of GM and LM3, but in any case not resulting in more than a 5% change with respect to the $J = 0$ case. The increase in kinetic energy is much bigger in the case of dissociation to methyl plus acetylene. The change is less than 10% for GM but goes up to about 20% for LM3 and over 50% for LM1 and LM2. Examination of individual "J*, no-coll" trajectories has permitted evaluation of the correlation between the kinetic energy and the orbital angular momentum of the dissociation products. For example, for dissociations to methyl + acetylene from LM2, the correlation has an R^2 of 0.55 and along the regression line the kinetic energy of the fragments increases by 0.168 kcal/mol per unit of orbital angular momentum. For dissociation to H + propyne from LM1, R^2 = 0.33 and the increase is 0.267 kcal/mol per unit of orbital angular momentum. For dissociation to H + allene from GM, R^2 = 0.21 and the increase is 0.209 kcal/mol per unit of orbital angular momentum.

Figure 14 summarizes the branching ratios of different products obtained after unimolecular dissociation of the allyl.

dx.doi.org/10.1021/jp5062013 | J. Phys. Chem. A 2014, 118, 7742−7757

By comparison of histograms for "J^*, no-coll", and "J, post-coll", we do not detect any substantial variation in the branching ratios. This means that even if, on average, it relaxes the molecule and subtracts angular momentum, a single collision is not enough to produce a clear effect on the branching ratios of the subset of trajectories dissociating during the 24 ps evolution that follows the collision. Likewise, addition of angular momentum has usually just a minor effect. A weak effect can be noticed for LM2 where rotation favors (1,3) elimination with respect to H + propyne or for LM1 with H + propyne advantaged over H + allene and (1,2) elimination. In these cases, the favored channels have the lowest barriers to dissociation. An increment in rotation leaves less energy available for overcoming such barriers, and the lowest open channels are favored. In any case, the general conclusion of our examination is that the relative distribution of products does not strongly depend either on initial rotation or on the single collision.

To focus on the effects of rotation on the isolated radical, in Table 7 we report detailed information for trajectories of the group "J^*, no-coll". Yield data have already been graphically presented in Figure 14. The table presents an estimate of the average initial rotational energy, based on the instantaneous rotational energy of the initial configuration of each trajectory. Even if this is just a rough estimate (we will discuss this point further in the final section), it can be useful from a qualitative point of view when making a comparison between the different dissociation channels. The average rotational energy data reveal that large values usually correspond to the trajectories which do not lead to any kind of dissociation. An exception is the (1,3) methyl channel for LM2, but in that case the potential barrier for dissociation is low compared to those for the other isomers (about 37 kcal/mol instead of 60−70 kcal/mol) and even if about 25% of excitation energy is confined in rotation, it remains a huge excess of energy available for dissociation via the (1,3) methyl channel. In general, with the just mentioned exception of LM2, H-elimination channels are favored with respect to methyl-elimination ones. Furthermore, Table 7 presents the average orbital angular momentum and average exit parameter calculated as $b = L/\mu v_{rel}$, where μ is the reduced mass. Data show that the average orbital angular momentum and exit parameter are bigger in the case of methyl elimination. H-elimination channels are characterized by a lower orbital angular momentum, partly due to the small hydrogen mass which acts as the reduced mass and partly due to the smaller average exit parameters.

Table 7. Name of Isomer, Dissociation Channel, Average Instantaneous Initial Rotational Energy (cm^{-1}), Dissociation Yield, Orbital Angular Momentum ($\hbar$), and Average Exit Parameter (au) for the "J^*, no-coll" Group

	channel	$\langle E^{rot,in}\rangle$	yield	$\langle L\rangle$	$\langle b\rangle$
GM	no diss	16 735	79.0	–	–
GM	H + allene	6138	17.5	24.6	1.4
GM	H + propyne	6181	2.5	31.4	2.0
GM	Meth(1,3)	3856	1.0	75.0	1.4
GM	Meth(1,2)	4536	∼0	98.9	2.4
LM1	no diss	21 726	19.8	–	–
LM1	H + allene	9274	24.0	32.1	1.8
LM1	H + propyne	11 254	51.4	32.2	2.1
LM1	Meth(1,2)	9033	4.8	116.6	2.9
LM2	no diss	8820	1.0	–	–
LM2	H + allene	3468	0.0	22.2	1.3
LM2	H + propyne	8282	8.9	24.1	1.7
LM2	Meth(1,3)	13 899	90.1	146.4	2.0
LM3	no diss	13 058	69.5	–	–
LM3	H + allene	7938	25.6	23.8	1.4
LM3	H + propyne	7848	3.6	27.9	1.9
LM3	Meth(1,3)	4672	1.2	71.6	3.2

As a final way to point out qualitatively the effect of rotation, we have investigated the dependence on internal excitation of unimolecular rate constants for $J = 0$. In fact, for a constant value of the total internal energy, when rotation is present the amount of energy available for dissociation is reduced with respect to the $J = 0$ case. This explains why dissociation times and the fraction of nonreactive trajectories increase when the molecule rotates. The dependence of unimolecular rate constants on available energy was estimated by running batches of $J = 0$ trajectories at different internal excitations. Rate constants were determined by means of dissociation yields and by fitting the undissociated molecule distribution vs time. RRKM calculations were performed for the main dissociation channels and provided results within a factor of 6 of trajectory estimates.

Figure 15 shows a plot of $\log_{10} k_{uni}$ as a function of the excitation above the GM energy. As an estimate, at a total energy of about 157 kcal/mol (≈ 55 000 cm^{-1}) all of the channels displayed fall in $\log_{10} k_{uni}$ by 0.2−0.6 units (k_{uni} falls by 37−75%) with a decrease in excitation energy of about 34 kcal/mol. The slope of the $\log_{10} k_{uni}$ vs excitation energy curve is generally lower for channels with low barriers than for channels with high barriers. This further justifies why the lowest open channels are favored when less energy is available to overcome the barriers.

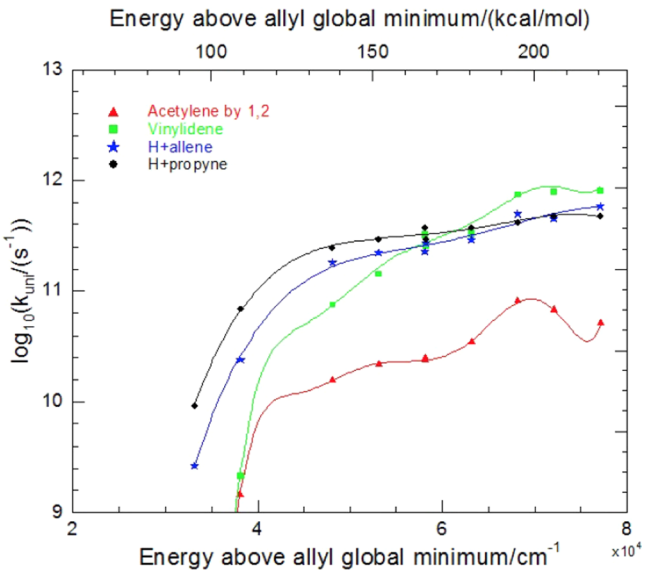

Figure 15. Dependence of unimolecular rate constants for different dissociation channels on the internal excitation energy ($J = 0$).

IV. DISCUSSION AND CONCLUSIONS

We have shown that initial rotation is very important for energy transfer and dissociation. Results are more affected by rotational angular momentum than by a single collision or by the type of starting isomer. Due to the different degree of

dx.doi.org/10.1021/jp5062013 | J. Phys. Chem. A 2014, 118, 7742−7757

quantization of molecular energy types, in weak collisions it seems quite reasonable to find that a larger fraction of rotational energy in the target molecule is correlated with higher transfer efficiency. Vibrational energy, on the other hand, is enabling configuration changes in the molecules, and it is thereby more directly related to reaction than rotational energy. There is angular momentum conservation in the isolated molecule, but if no rigorous separation of internal molecular energies is present, then a collision with an argon atom can both cause energy transfer and internal relaxation toward microcanonical equilibrium.

In an attempt to discuss in more detail some important aspects, we start by discussing whether the initial excitation (about 157 kcal/mol) can be rigorously partitioned between rotation and vibration. The allyl in its equilibrium configuration is an asymmetric rotor, characterized by three different moments of inertia and three different rotational constants, with one of them much bigger than the other two (see Table 8). There is no closed form available for term values of an asymmetric top, so it is not possible to rigorously rely on a well-defined mathematical relation between E^{rot} and the magnitude J of the rotational angular momentum. An approximate partition could have been obtained by considering the allyl as a symmetric top (taking one of the constants as equal to the average between the two smallest ones for the asymmetric top) and by considering the associated rotational constants of the equilibrium configuration as independent of time.[52] However, at the high excitation energy employed here, rovibrational coupling realistically plays an important role and the separation breaks down. Furthermore, the molecular structure undergoes wide deformations. This is clear from Figure 16, where the time dependence of the rotational constants (right panels) has been followed for a total time of 3 ps. The values of rotational constants averaged over the trajectory are reported in the caption of Figure 16 and show differences of about 5−10% from the equilibrium constants. The latter are presented for all isomers in Table 8. In the last column of Table 8, the "spherical" rotational constants are reported. They are used by our model for energy transfer[59] and calculated from the "spherical" moment of inertia $I = 2/3\sum m_i r_i^2$, where r_i indicates the distance of the i-th atom from the allyl center of mass.

Table 8. Equilibrium and Spherical Rotational Constants (in cm^{-1}) for the Four Isomers

	A_{eq}	B_{eq}	C_{eq}	B_{sph}
GM	1.822	0.346	0.291	0.437
LM1	2.349	0.294	0.274	0.401
LM2	1.897	0.322	0.289	0.424
LM3	0.782	0.697	0.448	0.607

Another possible strategy for partitioning rotational and vibrational energy would have been to estimate the rotational energy instantaneously with the classical formula $E^{rot} = (1/2) I\omega^2$. This is the formula we have used to get a rough estimate of the average initial rotational energy reported in Table 7. During the motion, this quantity oscillates in an irregular way (converting back and forth between vibrational and rotational energy) as shown from its time dependence in Figure 16 (left panel). The instantaneous value is not suitable for quantifying precisely and univoquely the rotational energy. For all these reasons, we have in general decided not to report a partition between rotational and vibrational energy.

However, Figure 17 shows that after a transient period of about 1 ps, the ensemble-averaged instantaneous rotational energy starts oscillating around a central "expectation" value, which could be used as an estimate for the rotational energy. Figure 17 has been obtained by averaging the evolution of the instantaneous rotational energy of the isolated allyl over a set of 60 different trajectories originated from GM geometry and characterized by a definite magnitude of the angular momentum ($J^* = 170\hbar$). The expectation value of this ensemble-averaged rotational energy is estimated to be about

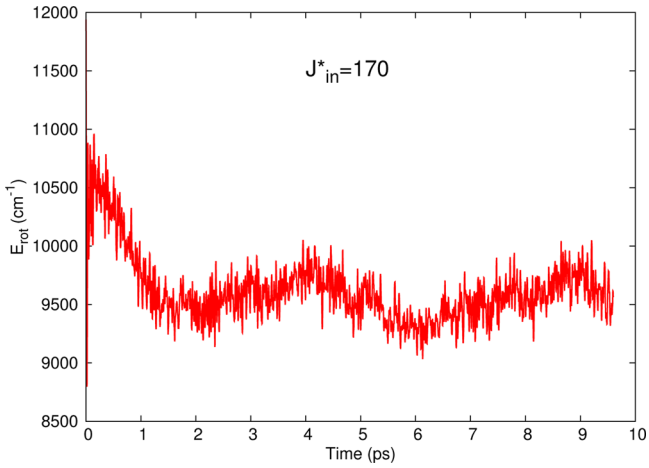

Figure 17. Instantaneous rotational energy averaged over 60 trajectories with angular momentum $J^* = 170\hbar$.

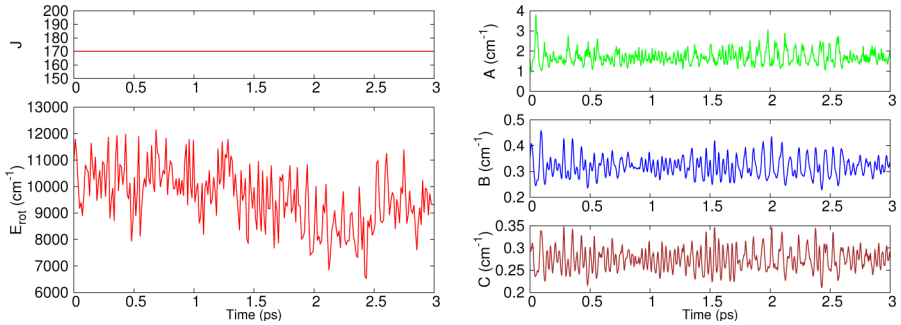

Figure 16. Angular momentum, instantaneous rotational energy, and rotational constants for an isolated allyl radical with internal excitation of about 157.2 kcal/mol (55 000 cm^{-1}) and $J^* = 170\hbar$ as a function of time. Rotational constants (in cm^{-1}) for the GM equilibrium geometry are $A_{eq} = 1.822$, $B_{eq} = 0.346$, and $C_{eq} = 0.291$, while the values averaged over the trajectory are $A = 1.625$, $B = 0.334$, and $C = 0.280$.

dx.doi.org/10.1021/jp5062013 | J. Phys. Chem. A 2014, 118, 7742−7757

9600 cm^{-1}. If the molecule is treated as a spherical rotor, the corresponding rotational constant is equal to 0.33 cm^{-1}, a value not far from those reported in Table 8. Our model adopts an effective rotational constant equal to 0.8 B_{sph} which gives a value of 0.35 cm^{-1} for the GM case.[59]

The transient-time dynamics in Figure 17 could affect also the effectiveness of our microcanonical sampling of the initial conditions. Our collisional trajectories at E_{coll} = 10 kcal/mol last on average less than 1 ps, and moreover, we have always started our simulations exactly from one of the four isomer geometries. If the advantages of this approach include, by starting in specified allyl geometries, the ability to make a comparison to our previous results for nonrotating allyl[6,7] and to directly evaluate isomer effects, the main drawback is that it may be questioned if there was enough time for the allyl to sample completely the phase space before the collision, in such a way that a fully microcanonical distribution had actually been achieved as desired. To check this question, we ran about 5000 additional collisions with the argon starting very far away (65 au) from the allyl, so that the radical had about 1.2 ps to evolve alone before starting to interact. The initial geometry for these additional trajectories was the GM one, and velocities were randomly sampled as previously described. Internal excitation and collision energy were also as before. The average total energy transfer for this new "long-distance" batch of trajectories is found to be −537 cm^{-1}, and the average energy transfer down, −1297 cm^{-1}. The difference is about 4% and 6% from data reported in Table 3. This means that microcanonical sampling in our simulations has been performed effectively.

Finally, in examining the effect of rotational angular momentum on the unimolecular dissociation, we have justified the results on the basis of the energy tied up in rotation and of the minor amount of internal excitation available for dissociation. Another way of describing the dissociation reactions is in terms of a centrifugal barrier. The potential energy of the system can be written as the sum of the potential in the absence of angular momentum plus a centrifugal barrier, whose value depends on the angular momentum J and the moment of inertia. The addition of the centrifugal potential makes it more difficult, at a fixed total internal energy, to overcome the barrier. As the molecule dissociates, the rotational energy decreases from its initial value because the moment of inertia increases as the dissociating bond is stretched. Whether one looks at the problem from the point of view of rotational energy that is not available for surmounting the barrier or from the point of view of a centrifugal barrier to dissociation that increases with rotation, the conclusion is that an increase in initial rotational energy for a constant total excitation energy is likely to decrease the rate of reaction channels.

To conclude, we remark that the physical quantities which can be rigorously calculated are the energy transfer and the variation in rotational angular momentum. In this study we have demonstrated that the addition of angular momentum can produce major effects concerning energy transfer and dissociation. Effects of a single collision with argon and dependence on the type of starting isomer can be detected and evaluated but have a minor impact on the outcomes of collisional and unimolecular trajectories. A model providing a physical explanation for collision activation and deactivation and interpretation of probability distributions is the topic of our upcoming paper in this Journal.

AUTHOR INFORMATION

Corresponding Authors

*E-mail: riccardo.conte@emory.edu.
*E-mail: paul.houston@cos.gatech.edu.
*E-mail: jmbowma@emory.edu.

Notes

The authors declare no competing financial interest.

ACKNOWLEDGMENTS

This material is based upon work supported by the U.S. Department of Energy, Office of Science, Office of Basic Energy Sciences, under Award Number DE-FG02-97ER14782.

REFERENCES

(1) Huchnall, D. J. *Chemistry of Hydrocarbon Combustion*; Chapman and Hall: London, 1985.

(2) Fernandes, R. X.; Giri, B. R.; Hippler, H.; Kachiani, C.; Striebel, F. Shock Wave Study on the Thermal Unimolecular Decomposition of Allyl Radicals. *J. Phys. Chem. A* **2005**, *109*, 1063−1070.

(3) Stranges, D.; Stemmler, M.; Yang, X.; Chesko, J. D.; Suits, A. G.; Lee, Y. T. UV Photodissociation Dynamics of Allyl Radical by Photofragment Translational Spectroscopy. *J. Chem. Phys.* **1998**, *109*, 5372−5382.

(4) Stranges, D.; O'Keeffe, P.; Scotti, G.; Di Santo, R.; Houston, P. L. Competing Sigmatropic Shift Rearrangements in Excited Allyl Radicals. *J. Chem. Phys.* **2008**, *128*, 151101/1−4.

(5) Chen, C.; Braams, B.; Lee, D. Y.; Bowman, J. M.; Houston, P. L.; Stranges, D. Evidence for Vinylidene Production in the Photodissociation of the Allyl Radical. *J. Phys. Chem. Lett.* **2010**, *1*, 1875−1880.

(6) Chen, C.; Braams, B.; Lee, D. Y.; Bowman, J. M.; Houston, P. L.; Stranges, D. The Dynamics of Allyl Radical Dissociation. *J. Phys. Chem. A* **2011**, *115*, 6797−6804.

(7) Conte, R.; Houston, P. L.; Bowman, J. M. Classical Trajectory Study of Energy Transfer in Collisions of Highly Excited Allyl Radical with Argon. *J. Phys. Chem. A* **2013**, *117*, 14028−14041.

(8) Ratliff, B. J.; Womack, C. C.; Tang, X. N.; Landau, W. M.; Butler, L. J.; Szpunar, D. E. Modeling the Rovibrationally Excited C_2H_4OH Radicals from the Photodissociation of 2-Bromoethanol at 193 nm. *J. Phys. Chem. A* **2010**, *114*, 4934−4945.

(9) Womack, C. C.; Ratliff, B. J.; Butler, L. J.; Lee, S.-H.; Lin, J. J.-M. Photoproduct Channels from $BrCD_2CD_2OH$ at 193 nm and the HDO + Vinyl Products from the CD_2CD_2OH Radical Intermediate. *J. Phys. Chem. A* **2012**, *116*, 6394−6407.

(10) McKown, B. G.; Ceriotti, M.; Womack, C. C.; Kamarchik, E.; Butler, L. J.; Bowman, J. M. Effects of High Angular Momentum on the Unimolecular Dissociation of CD_2CD_2OH: Theory and Comparisons with Experiment. *J. Phys. Chem. A* **2013**, *117*, 10951−10963.

(11) Szpunar, D. E.; Morton, M. L.; Butler, L. J.; Regan, P. M. Primary and Secondary Dissociation from Allyl Iodide Excited at 193 nm: Centrifugal Effects in the Unimolecular Dissociation of the Allyl Radical. *J. Phys. Chem. B* **2002**, *106*, 8086−8095.

(12) Szpunar, D. E.; Liu, Y.; McCullagh, M. J.; Butler, L. J.; Shu, J. Photodissociation of allyl-d_2 iodide excited at 193 nm: Stability of highly rotationally excited H_2CDCH_2 radicals to C−D fission. *J. Chem. Phys.* **2003**, *119*, 5078−5084.

(13) Lindemann, F. A. Discussion on the Radiation Theory of Chemical Action. *Trans. Faraday Soc.* **1922**, *17*, 598−599.

(14) Christiansen, J. A.; Kramers, H. A. Velocity of Chemical Reactions. *Z. Phys. Chem.* **1923**, *104*, 451−471.

(15) Löhmannsröben, H. L.; Luther, K. Selective Multiphoton Ionization in Dense Manifolds of Vibrational States. *Chem. Phys. Lett.* **1988**, *144*, 473−478.

(16) Mullin, A. S.; Michaels, C. A.; Flynn, G. W. Molecular Supercollisions: Evidence for Large Energy Transfer in the Collisional

Relaxation of Highly Vibrationally Excited Pyrazine by CO_2. *J. Chem. Phys.* **1995**, *102*, 6032−6045.
(17) Weston, R. E., Jr.; Flynn, G. W. Relaxation of Molecules with Chemically Significant Amounts of Vibrational Energy: The Dawn of the Quantum State Resolved Era. *Annu. Rev. Phys. Chem.* **1992**, *43*, 559−589.
(18) Hippler, H.; Lindemann, L.; Troe, J. Collisional Energy Transfer of Vibrationally Highly Excited Molecules. V. UV Absorption Study of Azulene. *J. Chem. Phys.* **1985**, *83*, 3906−3912.
(19) Oref, I.; Tardy, D. C. Energy Transfer in Highly Excited Polyatomic Molecules. *Chem. Rev.* **1990**, *90*, 1407−1445.
(20) Flynn, G. W.; Parmenter, C. S.; Wodtke, A. M. Vibrational Energy Transfer. *J. Phys. Chem.* **1996**, *100*, 12817−12838.
(21) Mullin, A. S.; Schatz, G. C.; Eds. *Highly Excited Molecules: Relaxation, Reaction and Structure*; ACS Symposium Series 678; American Chemical Society: Washington, DC, 1996.
(22) Hold, U.; Lenzer, T.; Luther, K.; Reihs, K.; Symonds, A. C. Collisional Energy Transfer Probabilities of Highly Excited Molecules from Kinetically Controlled Selective Ionization (KCSI). I. The KCSI Technique: Experimental Approach for the Determination of P(E′,E) in the Quasicontinous Energy Range. *J. Chem. Phys.* **2000**, *112*, 4076−4089.
(23) Grigoleit, U.; Lenzer, T.; Luther, K.; Mützel, M.; Takahara, A. Collisional Energy Transfer of Highly Vibrationally Excited Toluene and Pyrazine: Transition Probabilities and Relaxation Pathways from KCSI Experiments and Trajectory Calculations. *Phys. Chem. Chem. Phys.* **2001**, *3*, 2191−2202.
(24) Hold, U.; Lenzer, T.; Luther, K.; Symonds, A. C. Collisional Energy Transfer Probabilities of Highly Excited Molecules from KCSI. III. Azulene: P(E′,E) and Moments of Energy Transfer for Energies up to 40,000 cm^{-1} via Self-calibrating Experiments. *J. Chem. Phys.* **2003**, *119*, 11192−11211.
(25) Liu, C.-L.; Hsu, H. C.; Hsu, Y. C. Energy Transfer of Highly Vibrationally Excited Naphtalene. I. Translational Collision Energy Dependence. *J. Chem. Phys.* **2007**, *127*, 104311/1−7.
(26) Du, J.; Sassin, N. A.; Havey, D. K.; Hsu, K.; Mullin, A. S. Full State-Resolved Energy Gain Profiles of CO_2 from Collisions with Highly Vibrationally Excited Molecules. II. Energy-Dependent Pyrazine (E = 32700 and 37900 cm^{-1}) Relaxation. *J. Phys. Chem. A* **2013**, *117*, 12104−12115.
(27) Wall, M. C.; Mullin, A. S. Supercollision" Energy Dependence: State-resolved Energy Transfer in Collisions Between Highly Vibrationally Excited Pyrazine (E_{vib} = 37,900 cm^{-1} and 40,900 cm^{-1}) and CO_2. *J. Chem. Phys.* **1998**, *108*, 9658−9667.
(28) Wall, M. C.; Lemoff, A. S.; Mullin, A. S. Independent Determination of Supercollision Energy Loss Magnitudes and Rates in Highly Vibrationally Excited Pyrazine with E_{vib} = 36,000−41,000 cm^{-1}. *J. Phys. Chem. A* **1998**, *102*, 9101−9105.
(29) Pashutzki, A.; Oref, I. Collision-induced Dissociation of Cyclohexadiene by a Vibrationally Hot Collider. *J. Phys. Chem.* **1988**, *92*, 178−182.
(30) Liu, C.-L.; Hsu, H. C.; Lyu, J.-J.; Ni, C.-K. Supercollisions and Energy Transfer of Highly Vibrationally Excited Molecules. *J. Chem. Phys.* **2005**, *123*, 131102/1−4.
(31) Gilbert, R. G. Theory of Collisional Energy Transfer of Highly Excited Molecules. *Int. Rev. Phys. Chem.* **1991**, *10*, 319−347.
(32) Clary, D. C.; Gilbert, R. G.; Bernshtein, V.; Oref, I. Mechanisms for Supercollisions. *Faraday Discuss.* **1995**, *102*, 423−433.
(33) Li, Z.; Sansom, R.; Bonella, S.; Coker, D. F.; Mullin, A. S. Trajectory Study of Supercollision Relaxation in Highly Vibrationally Excited Pyrazine and CO_2. *J. Phys. Chem. A* **2005**, *109*, 7657−7666.
(34) Miller, L. A.; Barker, J. R. Collisional Deactivation of Highly Vibrationally Excited Pyrazine. *J. Chem. Phys.* **1996**, *105*, 1383−1391.
(35) Lendvay, G.; Schatz, G. C. Energy Dependence of Energy Transfer in the Collisional Relaxation of Vibrationally Highly Excited CS_2. *J. Phys. Chem.* **1991**, *95*, 8748−8753.
(36) Lim, K. F. Quasiclassical Trajectory Study of Collisional Energy Transfer in Toluene Systems. I. Argon Bath Gas: Energy Dependence and Isotope Effects. *J. Chem. Phys.* **1994**, *100*, 7385−7399.
(37) Lim, K. F. Quasiclassical Trajectory Study of Collisional Energy Transfer in Toluene Systems. II. Helium Bath Gas: Energy and Temperature Dependences, and Angular Momentum Transfer. *J. Chem. Phys.* **1994**, *101*, 8756−8767.
(38) Bruehl, M.; Schatz, G. C. Theoretical Studies of Collisional Energy Transfer in Highly Excited Molecules: Temperature and Potential Surface Dependence of Relaxation in He, Ne, Ar + CS_2. *J. Phys. Chem.* **1988**, *92*, 7223−7229.
(39) Bernshtein, V.; Lim, K. F.; Oref, I. Temporal Dependence of Collisional Energy Transfer by Quasiclassical Trajectory Calculations of the Toluene−Argon System. *J. Phys. Chem.* **1995**, *99*, 4531−4535.
(40) Meroueh, O.; Hase, W. L. Collisional Activation of Small Peptides. *J. Phys. Chem. A* **1999**, *103*, 3981−3990.
(41) Lenzer, T.; Luther, K.; Troe, J.; Gilbert, R. G.; Lim, K. F. Trajectory Simulations of Collisional Energy Transfer in Highly Excited Benzene and Hexafluorobenzene. *J. Chem. Phys.* **1995**, *103*, 626−641.
(42) Lendvay, G.; Schatz, G. C. Observation of Highly Energetic Collisions in Classical Trajectory Studies of Collisional Energy Transfer. *J. Phys. Chem.* **1990**, *94*, 8864−8866.
(43) Han, Y.-C.; Sharma, A. R.; Bowman, J. M. Quasiclassical Trajectory Study of Fast H-atom Collisions with Acetylene. *J. Chem. Phys.* **2012**, *136*, 214313/1−6.
(44) Lendvay, G.; Schatz, G. C. Comparison of Master Equation and Trajectory Simulation of the Relaxation of an Ensemble of Highly Vibrationally Excited Molecules. *J. Phys. Chem.* **1994**, *98*, 6530−6536.
(45) Martínez-Núñez, E.; Vázquez, S. A.; Marques, J. M. C. Quasiclassical Trajectory Study of the Collision-Induced Dissociation of CH_3SH^+ + Ar. *J. Chem. Phys.* **2004**, *121*, 2571−2577.
(46) Martínez-Núñez, E.; Fernández-Ramos, A.; Vázquez, S. A.; Marques, J. M. C.; Xue, M.; Hase, W. L. Quasiclassical Dinamycs Simulation of the Collision-Induced Dissociation of $Cr(CO)_6^+$ with Xe. *J. Chem. Phys.* **2005**, *123*, 154311/1−9.
(47) Pan, B.; Bowman, J. M. Quantum Scattering Calculations of Energy Transfer and Dissociation of HCO in Collisions with Ar. *J. Chem. Phys.* **1995**, *103*, 9661−9668.
(48) Qi, J.; Bowman, J. M. Quantum Calculations of Inelastic and Dissociative Scattering of HCO by Ar. *J. Chem. Phys.* **1998**, *109*, 1734−1742.
(49) Dagdigian, P. J.; Alexander, M. H. Exact Quantum Scattering Calculations of Transport Properties: CH_2−He. *J. Chem. Phys.* **2013**, *138*, 164305/1−7.
(50) Kieran, F. L.; McCormack, D. A. The conservation of quantum zero-point energies in classical trajectory simulations. *J. Chem. Phys.* **1995**, *102*, 1705−1715.
(51) Czako, G.; Kaledin, A.; Bowman, J. M. A practical method to avoid zero-point leak in molecular dynamics calculations: Application to the water dimer. *J. Chem. Phys.* **2010**, *132*, 164103/1−6.
(52) Jasper, A. W.; Miller, J. A. Collisional Energy Transfer in Unimolecular Reactions: Direct Classical Trajectories for $CH_4 \rightleftarrows CH_3$ + H in Helium. *J. Phys. Chem. A* **2009**, *113*, 5612−5619.
(53) Jasper, A. W.; Miller, J. A. Theoretical Unimolecular Kinetics for CH_4 + M $\rightleftarrows$ CH_3 + H + M in Eight Baths, M = He, Ne, Ar, Kr, H_2, N_2, CO, CH_4. *J. Phys. Chem. A* **2011**, *115*, 6438−6455.
(54) Jasper, A. W.; Miller, J. A.; Klippenstein, S. J. The Collision Efficiency of Water in the Unimolecular Reaction CH_4 (+H_2O) → CH_3 + H (+H_2O): One-Dimensional and Two-Dimensional Solutions of the Low-Pressure-Limit Master Equation. *J. Phys. Chem. A* **2013**, *117*, 12243−12255.
(55) Varandas, A. J. C.; Rodrigues, S. P. J. Double Many-Body Expansion Potential Energy Surface for Ground-State HCN Based on Realistic Long Range Forces and Accurate *Ab Initio* Calculations. *J. Chem. Phys.* **1997**, *106*, 9647−9658.
(56) Rodrigues, S. P. J.; Varandas, A. J. C. Dynamics Study of the Reaction Ar + HCN → Ar + H + CN. *J. Phys. Chem. A* **1998**, *103*, 6266−6273.
(57) Lauzin, C.; Coudert, L. H.; Herman, M.; Lievin, J. Ab Initio Intermolecular Potential of Ar-C_2H_2 Refined Using High- Resolution Spectroscopic Data. *J. Phys. Chem. A* **2013**, *117*, 13767−13774.

(58) Conte, R.; Houston, P. L.; Bowman, J. M. Communication: A benchmark-quality, full-dimensional ab initio potential energy surface for Ar−HOCO. *J. Chem. Phys.* **2014**, *140*, 151101/1−5.
(59) Houston, P. L.; Conte, R.; Bowman, J. M. Collisional Energy Transfer in Highly Excited Molecules, DOI: 10.1021/jp506202g.
(60) Hase, W. L. Classical Trajectory Simulations: Initial Conditions, a Chapter in Encyclopedia of Computational Chemistry, Vol. *1*; Allinger, N. L., Ed.; Wiley: New York, NY, 1998; pp 402−407.
(61) Porter, R. N.; Raff, L. M. In *Dynamics of Molecular Collisions*; Miller, W. H., Ed.; Plenum: New York, 1976; Vol. B.
(62) Nordholm, S.; Freasier, B. C.; Jolly, D. L. Ergodic Collision Theory of Intermolecular Energy Transfer. *Chem. Phys.* **1977**, *25*, 433−449.
(63) Börjesson, L. E. B.; Nordholm, S.; Andersson, L. L. Quantized Vibrational Densities of States and Ergodic Energy Transfer in Molecular Collisions. *Chem. Phys. Lett.* **1991**, *186*, 65−72.
(64) Ming, L.; Davidsson, J.; Nordholm, S. Energy transfer in collisions of small gas phase clusters. Comparison of molecular dynamics and statistical limit estimates. *Chem. Phys.* **1995**, *201*, 121−140.
(65) Nilsson, D.; Nordholm, S. Statistical model of energy transfer in molecular collisions: De-energization of highly excited toluene. *J. Chem. Phys.* **2002**, *116*, 7040−7048.
(66) Nilsson, D.; Nordholm, S. Statistical Theory of Collisional Energy Transfer in Molecular Collisions. *trans*-Stilbene Deactivation by Argon, Carbon Dioxide, and *n*-Heptane. *J. Phys. Chem. A* **2006**, *110*, 3289−3296.
(67) Ming, L.; Davidsson, J.; Nordholm, S. Molecular dynamics study of energy transfer in binary collisions of water molecules. *J. Chem. Phys.* **1996**, *104*, 9001−9015.
(68) Lenzer, T.; Luther, K.; Reihs, K.; Symmonds, A. C. Collisional energy transfer probabilities of highly excited molecules from kinetically controlled selective ionization (KCSI). II. The collisional relaxation of toluene: P(E′,E) and moments of energy transfer for energies up to 50,000 cm^{-1}. *J. Chem. Phys.* **2000**, *112*, 4090−4110.